Theoretical Design of Inkjet Process to Improve Delivery Efficiency

Y. Zhong[1], X. Dong[1], Z. Yin[2] and H. Fang[1][†]

[1] School of Energy and Power Engineering, Huazhong University of Science & Technology, Wuhan, Hubei, 430074, China
[2] School of Mechanical Science and Engineering, Huazhong University of Science & Technology, Wuhan, Hubei, 430074, China

†*Corresponding Author Email: hafang@hust.edu.cn*

ABSTRACT

Inkjet technology is an essential tool for precise and quick delivery of liquids in micro-droplets. A key topic of the technology is to deliver the droplets efficiently by designing the nozzle that is related to the droplet speed and the droplet volume in a stable inkjet process. The ejected droplets are usually too small to determine their physical states through onsite measurement. Complex physical phenomena, such as the coupling effects of surface tension, viscous force and inertial force, make it difficult to optimize the nozzle design by experiments alone. In the paper, we adopt computational fluid dynamics to investigate the inkjet process with the orthogonal test method to arrange the studied cases. The computational results firstly have been verified through measuring a simulated case that could be observed in the experiment. Different nozzle structures then have been examined by numerical simulation. It is found that the Laval-shaped nozzle can improve the droplet speed significantly to deliver the droplets fast, and that the curvilinear-triangle-shaped nozzle can minimize the droplet volume to improve the printing accuracy. It is further revealed that a large ink viscosity and surface tension, as well as a low ink density can improve the process stability. Additionally, a parameter combined by the droplet speed, the droplet volume and the stability level is proposed to evaluate the comprehensive performance of the inkjet nozzle.

Keywords: Inkjet technology; Physical properties; Droplet delivery; Nozzle design.

1. INTRODUCTION

Inkjet technology has come into the public limelight for over a century, and till now it is efficiently utilized in numerous fields including additive manufacturing(Zhang *et al.,* 2018), electronic devices(Liao *et al.,* 2018)(Khan *et al.,* 2015) and biotechnology(Tse and Smith, 2018)(Infanger *et al.,* 2019). One of the remaining challenges in this technology is how to deliver the ink stably and fast in a small volume, which determines the printing resolution and the ink consumption. During the past decades, researchers have focused on the mechanism analysis with linear and nonlinear instability theories, and on the external regulation of the printing parameters including advanced materials and their applications. Keller *et al.* (1973) showed that small perturbation resulting in collapse of cylinder liquid jet is not uniform, and its growth rate keeps increasing. Peregrine (1972) first

proposed the lubrication theory to explain a distinctive nonlinear phenomenon different from the classic wavelength prediction. Barenblatt (1996) presented in nonlinear theory the self-similarity to solve the singularity problem. Eggers and Dupont (Eggers, 1993) (Eggers and Dupont 1994) extended the theories to practical 3D cases. Martínez-Calvo (2018) conducted experimental and theoretical studies regarding nonlinear mechanics of viscous fluid, and pointed out that the available range of droplet ejection varies with the flow rate and the flow velocity.

The newly developed inkjet technologies have demonstrated their precise control capability of droplets (Castrejon-Pita *et al.,* 2013), for example, the acoustic drop generation (Elrod *et al.,* 1989) (Hadimioglu *et al.* n.d.) and cavity collapse (Silverbrook, 2011) methods. Rosati *et al.* (2019) designed an inkjet-printed flexible biosensor for rapid label-free antibiotic detection. Kastner *et al.,*
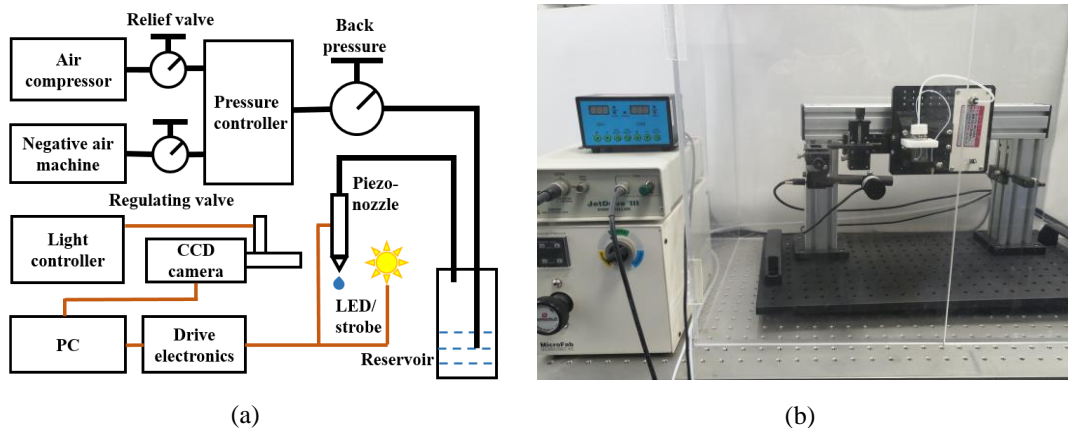
Fig. 1. (a) Schematic diagram of the experimental process, and (b) the experimental devices.

(2019) introduced a new method for production of printable graphene flakes applied in organic solar cells. These newly techniques have urged a complete study of the nozzle design to obtain accurate, fast and stable inkjet process. To obtain the optimal operating parameters, Lin and Reitz (1998) reviewed mechanisms of droplet ejection, and developed a method with separate regions of inkjet dependent on shapes and conditions. Chen and Basaran (2002) applied a new piezoelectric waveform to balance the surface tension, the viscous force and the inertial force, and greatly reduced the radius of droplets without change of the nozzle diameter. McGuinness *et al.* (2005) designed a three-dimensional nozzle to reduce volume of the droplets through numerical surface minimization according to Chen and Brenner (2004). Mishra *et al.* (2010) proposed a pulsed DC voltage signal to produce fast and accurate electro-hydrodynamic jet simultaneously. Shimobayashi *et al.* (2018) adopted sugar-assisted depinning of the contact line to suppress the coffee-ring effect. Wijshoff (2018) discussed the physics behind inkjet printing process by experimental and numerical techniques, and provided means of recording very fast micrometer-sized droplets with small disturbances. Stability criteria are developed in order to judge the performance of the inkjet process. Fromm (1984) first introduced a dimensionless criterion Z, the ratio of Reynold number to Weber number, and indicated that a liquid with the Z number larger than 2 could be ejected stably. Reis and Derby (2000) recommended the stable range of Z from 1 to 10. Choi *et al.* (2015) extended the stable range to 0.23~84. Recently, Zhong *et al.* (2018) developed a more applicable criterion named Pj that combines the driving parameters and the ink properties to evaluate a stable inkjet process.

Regarding the nozzle design, however, the influencing parameters have not been comprehensively investigated. Specially, the coupled influence of the nozzle structure and the fluid properties has been seldom discussed. Additionally, lack of an efficiently optimized method of the inkjet nozzle design critically limits the new inkjet techniques. In the current study, we conducted computational simulation based on experimental measurement on the nozzle performance, characterized by the droplet volume, the droplet velocity, and the process stability, and finally proposed a strategy based on the orthogonal test method to choose the nozzle and to design the ink.

2. EXPERIMENTAL SETUP

A drop-on-demand inkjet apparatus, as shown in Fig. 1, is adopted for visualizing the process of droplet ejection, and further for validating the numerical model. This system contains a droplet generation module and a visual observation module. The former includes an air compressor, a negative air machine, a precise pressure controller, a reservoir, drive electronics, a computer, a piezo-nozzle and multiple valves. The nozzle used in the study is a MJ-AT-01 piezo-nozzle manufactured by Microfab Company with a diameter of 80 μm. The pressure controller output a backpressure into the upper space of the reservoir, which makes the liquid inside the nozzle horizontal by balancing the pressures inside and outside the nozzle. With the pulse triggered by the driving electronics input by a computer, the piezoelectric element controls deformation of the quartz nozzle's wall to generate a droplet. The visual observation module including a CCD camera, a LED/strobe and a light controller, captures pictures of the moving droplets with a serial of delayed images. The CCD camera works with a frame rate of 22 fps, a single pixel size of 3.75 μm, and an effective pixel of 1280*960. It equips a quadruple magnifier with a focal distance of 65 mm. The exposure time for the LED/strobe is approximately 5 μs to preclude "smearing" effect along the trajectory.

3. PHYSICAL AND MATHEMATICAL MODELS

The inkjet process includes the actuation stage, the droplet formation stage, and the droplet motion stage. A long ink channel with a nozzle at the right side and a large reservoir at the left side is
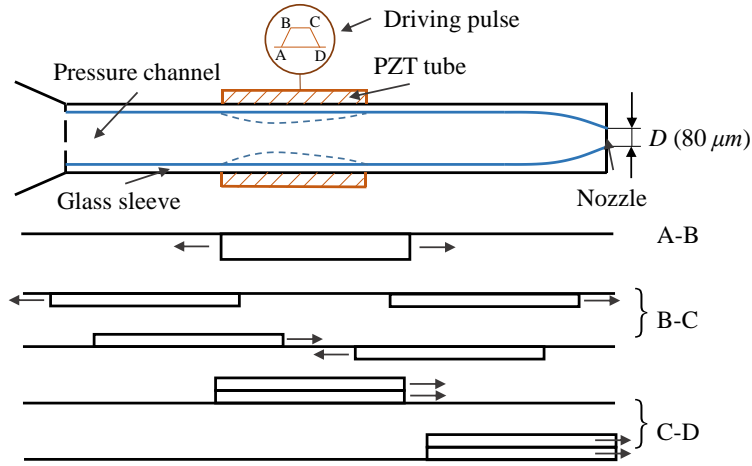
Fig. 2. Structure of the piezo-nozzle and schematic drawing of the actuation principle.

simplified as the geometry shown in Fig. 2. To generate a droplet, a driving pulse is applied and the PZT tube is deformed by the piezoelectric effect. The first slope of the driving pulse (A-B) enlarges the channel and causes a negative pressure wave, which propagates in two opposite directions with half of the amplitude. Half of the negative pressure wave is reflected after it meets with the nozzle end, while the other half one becomes a positive pressure wave after reflection at the reservoir. When the de-charging is applied (C-D), the positive pressure wave is amplified so that a large incoming positive pressure peak arrives at the nozzle to push the ink out. The actuation stage depends on the size of the channel and the speed of sound. However, the effect of compressibility of fluid is neglected during simulation according to the narrow channel theory (Wijshoff, 2010). After the ink is pushed out, a jet is formed. The bottom of the jet moves with large velocity, and it drags a long tail along. As the pressure near the break off point approaches infinity, the tail breaks off after tens of milliseconds creating a long tail. This stage is named as the droplet formation stage. Due to the uneven distribution of pressure within the falling droplet, the droplet oscillates in the air with certain oscillation period. The degree of the droplet oscillation decreases with the increase of falling distance, and the droplet ends up with sphere. However, the oscillation may not be completely damped before the droplet deposits on the substrate. So the initial state of the droplet motion stage has great impact on printing precision. The commercial software COMSOL is adopted to realize this process. The droplet moving speed in our study is generally up to 20 m/s, viz. the Re number is generally below 2000, hence the flow is considered as laminar flow. To model the details of the generation of droplets, the incompressible Navier-Stokes (N-S) equations are adopted for calculating the liquid flows:

$$\rho(\frac{\partial \mathbf{u}}{\partial t} + \mathbf{u} \cdot \nabla \mathbf{u}) - \mu \Delta \mathbf{u} + \nabla p = \mathbf{F}_{st} \tag{1}$$

$$(\nabla \cdot \mathbf{u}) = 0 \tag{2}$$

where ρ is the density, $\boldsymbol{\mu}$ is the dynamic viscosity, $\mathbf{u}$ is the velocity vector, p is the pressure, and $\mathbf{F}_{st}$ is the surface tension force, which is expressed by

$$\mathbf{F}_{st} = \nabla \cdot \mathbf{T} \tag{3}$$

$$\mathbf{T} = \sigma(\mathbf{I} - (\mathbf{nn}^T))\delta \tag{4}$$

where $\mathbf{T}$ is the stress tensor, $\mathbf{n}$ is the interface normal, σ is the surface tension coefficient, and δ is the Dirac delta function which is zero except at the fluid interface. The interface normal is defined as

$$\mathbf{n} = \frac{\nabla \Phi}{|\nabla \Phi|} \tag{5}$$

The delta function can be calculated by

$$\delta = 6|\Phi(1-\Phi)||\nabla_{\Phi}| \tag{6}$$

where Φ is the level set function, and a contour of $\Phi=0.5$ is considered as the interface between liquid and air. The level set method is proper for tracing the free surface with adaptive meshing during calculation. A reinitialization process is included in the calculation for better convergence (Olsson and Kreiss, 2005)(Olsson *et al.,* 2007). The convection for the reinitialized level set function can be described as

$$\frac{\partial \Phi}{\partial t} + \nabla \cdot (\Phi \mathbf{u}) + \gamma[(\nabla \cdot (\Phi(1-\Phi)\frac{\nabla \Phi}{|\nabla \Phi|})) \\ - \varepsilon \nabla \cdot \nabla \Phi] = 0 \tag{7}$$

where γ and ε denotes the maximum magnitude of velocity and the thickness of the transition layer respectively. Properties of density and viscosity across the interface are related to Φ as

$$\rho = \rho_{air} + (\rho_{ink} - \rho_{air})\Phi \tag{8}$$

$$\mu = \mu_{air} + (\mu_{ink} - \mu_{air})\Phi \tag{9}$$

Through providing an inlet velocity at the top, liquid is pushed out of the nozzle orifice to form the droplets. For simulation cases described below, the unstated parameters are fixed as 1.375 m/s for the inlet velocity, 10 μs for the pulse width and 80 μm for the equivalent diameter. The inlet condition is given as a velocity varied by time and radius,

$$v(r)=4V_{in}(\frac{r+0.1\text{mm}}{0.2\text{mm}})(1-\frac{r+0.1\text{mm}}{0.2\text{mm}})\text{m/s} \quad (10)$$

where V_{in} is a given constant velocity, r is the radial

position. The profile of velocity along the radius is parabolic as shown in Eq. (10) due to the viscous force. With a trapezoid pulse exerted, the inlet velocity is calculated by the following formulation,

$$v(r,t)=(\text{step}(t-1\cdot10^{-6}\text{s})$$
$$-\text{step}(t-(dt+3\cdot10^{-6})\text{s}))\cdot v(r) \quad (11)$$

where step(t) is a step function, and t is time. $v(r,t)$ first increases, and then decreases to approximate the actual pulse in experiments. The outlet is set as a constant pressure, and the walls abide by the non-slip conditions.

Prior studies of effects of wall shapes on droplet volume and speed are conducted by the 2D axisymmetric model with the average grid number of 4e4. Other cases are run in the 3D geometry with the average grid number of 2.5e5. A convergent study has been carried out to obtain mesh-independent results. The droplet's mass is chosen for comparison. When the grids are doubled, the droplet's mass change keeps within 1%. Hereby it is concluded that the simulation outcomes are insensitive to the grids.
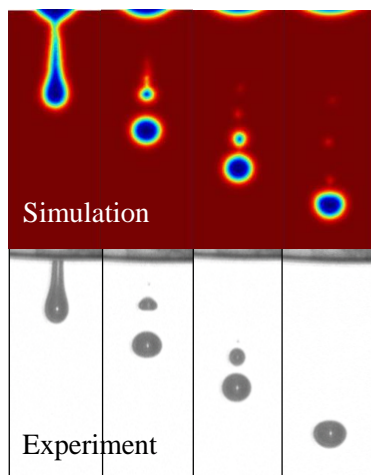

Fig. 3. Comparison of experimental and numerical results.

4. RESULTS AND DISCUSSION

4.1 Experimental verification

For experimental verification, images of both experiment and simulation are presented in Fig. 3.

A mixture of Ethanol and Glycerol (200:1) is applied for both experiment and simulation. In simulation V_{in} is set to 1.125 m/s, and in experiment the pulse amplitude is set to 40 V. Since it is more convenient to use a velocity inlet condition than to apply a driving pulse in simulations, the inlet velocity is employed as the driving force in simulations replacing the pulse amplitude in experiments. The obtained velocity profile at the nozzle outlet by time in experiments are summarized into a velocity profile for simulation, which makes the simulation and experiment results consistent. Time interval for both simulation and experiment is 60 μs. The droplet moving speed for simulation and experiment are 0.76 m/s and 0.78 m/s, respectively. From Fig. 3, it is obvious that a long jet is formed, and broke into a major droplet and a satellite. The satellite chases after the primary droplet with a faster speed. Then, the satellite and the primary droplet merge into a single droplet. The numerical pattern of the moving process of droplets matches that in experimental observation. The applied models and assumptions, therefore, are reliable for the following studies.

4.2 Analysis of Improved Nozzle Structure

As mentioned before, the volume and speed of droplet are two determinants that determine the precision and speed of inkjet process. In this part, we conduct studies about the elementary nozzle shapes including outlet shapes and wall shapes in order to seize the optimal nozzle structures that can achieve high droplet speed and small droplet volume, respectively.

As shown in Fig. 4, the elementary nozzle structures are enumerated. Among six types of nozzle outlet shape, a circular outlet is chosen mostly in real applications due to its manufacturing convenience. However, it generates droplets with maximum volume under the same applied pressure compared to other outlet nozzle shapes. Investigations of axis-switching oscillations in elliptical liquid jets help enhance the comprehensive understanding on instability theory (Wang and Fang, 2015). The droplet volume can be reduced by adopting other non-circular outlet nozzles, especially a nozzle shape that is roughly triangular with somewhat stretched out corners (Chen and Brenner, 2004). For the various outlet designs, the equivalent diameters D are set to a constant value of 80 μm. For the different walls, the outlet shapes are circular with the diameter of 80 μm as well.

In terms of previous tests, the effect of outlet shapes on improving droplet speed is minor compared with that of wall shapes. The effect of wall shapes on the droplet volume is also negligible compared with that of outlet shapes. Hence, Fig. 5 only exhibits variations of droplet moving speed when adopting various outlet shapes, and variations of droplet volume when adopting different wall shapes. The surface of droplet is determined by the Young-Laplace equation $p=\gamma K$, where p is the pressure difference across the fluid/air interface, γ is the surface tension, and K is the mean curvature of the
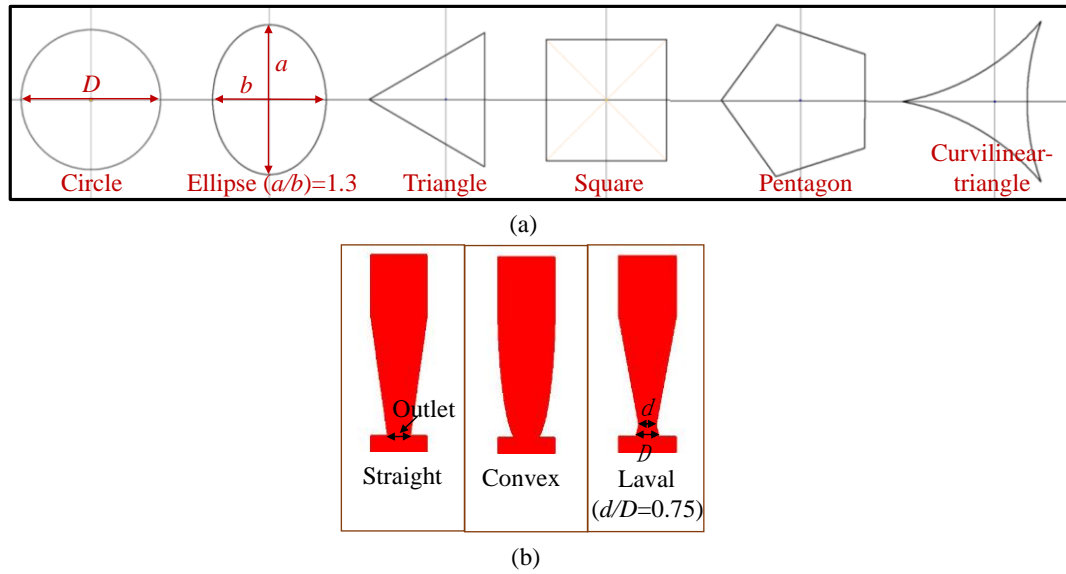
(a)

(b)

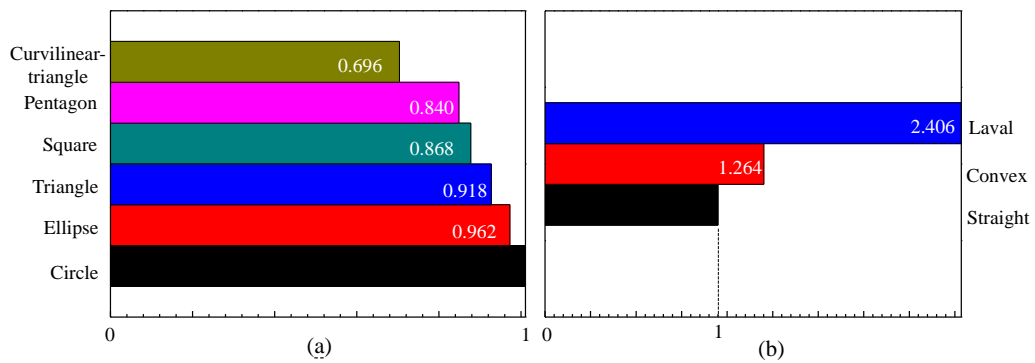**Fig. 4. The elementary nozzle shapes: (a) outlet shapes, and (b) wall shapes.**

Fig. 5. Rescaled and normalized droplet volume for (a) different outlets, and the speed for (b) different walls.

droplet surface. The boundary of the droplet surface is the nozzle edge. Droplets are ejected when the fluid inside the channel overcomes the surface tension at the nozzle. Hence, droplets generated from nozzles with larger mean curvature (meaning smaller surface tension to overcome) have smaller volume. In this regard, the curvilinear-triangle (CT) nozzle (with largest mean curvature of nozzle edge) shows best performance in reducing droplet volume. In the case of the curvilinear-triangle (CT) nozzle as presented in Fig. 5(a), the droplet volume is reduced by 30.4% in comparison with that of the circular nozzle. This outcome of volume optimization is consistent with the results from McGuinness *et al.* (2005).

Three candidate nozzles with different wall shapes are presented in Fig. 4(b). Nozzles with straight wall shape are commonly adopted. However, during the fabrication of the glass nozzles, the convex wall shape may appear. A structure that contracts and then expands has great impact on increasing liquid velocity and thus increasing the droplet speed

according to the continuity equation. Hereby, all three nozzle structures are conducted in simulation with the same inlet condition. Figure 5(b) indicates a dramatic increase of droplet speed by 140.6% when adopting the Laval nozzle, which results from the Laval effect. A nozzle structure with convex wall shape also gives rise to an increase of droplet speed by 26.4%, which attributes to the augment of the fluid volume inside the channel. From the two-dimensional study, the CT nozzle is best for droplet volume optimization. Adopting the Laval wall shape nozzle can increase the droplet speed largely. An extremely high speed can be obtained if D/d (see Fig. 4 for the dimensions) becomes infinity.

4.3 Optimization and Stability Analysis

As discussed above, the CT nozzle and the Laval nozzle are chosen nozzle structures for decreasing droplet volume and increasing droplet speed, respectively. We further use the two nozzle structures to investigate the effects of ink properties and the nozzle diameter on the droplet speed, droplet volume and process stability. In this part,

Table 1 Influencing factors of droplet ejection arranged for orthogonal analysis

Factors	Levels			Unit
	1	2	3	
A, Density	1000	1500	2000	kg/m³
B, Viscosity	1	15	30	cp
C, Surface tension	0.03	0.05	0.07	N/m
D, Diameter	40	60	80	μm

Table 2 Orthogonal table of L9-3-4 for the circular nozzle, and simulation results of the cases

Case	Density	Viscosity	Surface tension	Diameter	Speed	Volume	Stability	*Sc*
1	1000	1	0.03	40	15.044	2.56	4	1.469
2	1000	15	0.05	60	4.415	2.65	3	0.555
3	1000	30	0.07	80	0	2.63	1	0
4	1500	1	0.05	80	2.43	2.72	2	0.447
5	1500	15	0.07	40	14.39	2.56	4	1.405
6	1500	30	0.03	60	4.63	2.66	3	0.580
7	2000	1	0.07	60	6.111	2.55	3	0.799
8	2000	15	0.03	80	2.242	2.74	2	0.409
9	2000	30	0.05	40	14.39	2.61	4	1.378

Table 3 Orthogonal table of L9-3-4 for the Laval nozzle, and simulation results of the cases

Case	Density	Viscosity	Surface tension	Diameter	Speed	Volume	Stability	*Sc*
1	1000	1	0.03	40	19.414	2.59	4	1.874
2	1000	15	0.05	60	8.503	2.65	3	1.070
3	1000	30	0.07	80	1.3008	2.72	1	0.478
4	1500	1	0.05	80	4.796	2.77	3	0.577
5	1500	15	0.07	40	21.80	2.60	4	2.096
6	1500	30	0.03	60	8.866	2.69	3	1.099
7	2000	1	0.07	60	13.372	2.72	4	1.230
8	2000	15	0.03	80	5.098	2.79	3	0.609
9	2000	30	0.05	40	21.56	2.63	4	2.050

Table 4 Orthogonal table of L9-3-4 for the CT nozzle, and simulation results of the cases.

Case	Density	Viscosity	Surface tension	Diameter	Speed	Volume	Stability	*Sc*
1	1000	1	0.03	40	15.875	2.46	4	1.613
2	1000	15	0.05	60	4.843	2.41	3	0.670
3	1000	30	0.07	80	0	2.49	1	0
4	1500	1	0.05	80	2.209	2.53	2	0.436
5	1500	15	0.07	40	14.321	2.50	4	1.432
6	1500	30	0.03	60	5.142	2.56	3	0.670
7	2000	1	0.07	60	6.0453	2.43	3	0.829
8	2000	15	0.03	80	2.371	2.54	2	0.466
9	2000	30	0.05	40	14.948	2.52	4	1.483

we only run numerical cases for the convenience of varying unilateral parameters. Through orthogonal test method, optimal combination of those influential factors can be obtained theoretically. In addition, a parameter *Sc* (the abbreviation of score) is proposed to define the comprehensive performance of the three significant characteristics (the droplet speed, the droplet volume and the process stability) in inkjet process. *Sc* is defined as

$$Sc = \frac{v}{V \cdot C} \tag{12}$$

where v represents the speed of droplet, V is the volume of droplet and C is the class number of stability.

It is noted that the combination of the fluid properties in the optimized case may not a real fluid but an ideal fluid related to the nozzle that can provide a direction for ink design.

To evaluate the process stability, a classification of the cases is arranged in Table 1. As shown in Fig. 6, Class 1 is non-droplet or single droplet, Class 2 is a major droplet with several satellite droplets, Class 3

Table 5 Statistical analysis and optimal combination for droplet moving speed

Parameters	Laval				CT			
	A	*B*	*C*	*D*	*A*	*B*	*C*	*D*
k1	9.739	12.527	11.126	20.925	6.906	8.043	7.796	15.048
k2	11.821	11.800	11.620	10.247	7.224	7.178	7.333	5.343
k3	13.342	10.576	12.158	3.732	7.788	6.789	6.789	1.527
R	3.604	1.951	1.032	17.193	0.882	1.007	1.007	13.521
Order	D>A>B>C				D>B=C>A			
Optimization	$A_3B_1C_3D_1$				$A_3B_1C_1D_1$			

Table 6 Statistical analysis and optimal combination for droplet volume

Parameters	Laval				CT			
	A	*B*	*C*	*D*	*A*	*B*	*C*	*D*
k1	2.653	2.693	2.690	2.607	2.453	2.473	2.520	2.493
k2	2.687	2.680	2.683	2.687	2.530	2.483	2.487	2.467
k3	2.713	2.680	2.680	2.760	2.497	2.523	2.473	2.520
R	0.060	0.013	0.010	0.153	0.077	0.05	0.047	0.053
Order	D>A>B>C				A>D>B>C			
Optimization	$A_1B_{2/3}C_3D_1$				$A_1B_1C_3D_2$			

is a major droplet with a column of satellite droplets, and Class 4 is an elongated jet. The values of the scanned operating parameters (the ink density, viscosity, surface tension and the nozzle diameter) are chosen in Table 1. Each factor has three levels. The selected orthogonal table of $L_9 4^3$, including four factors and three levels, is adopted to arrange a systematic analysis. Simulated results about the droplet speed, volume and process stability using the circular, Laval and CT nozzles are presented in Tables 2-4, respectively.
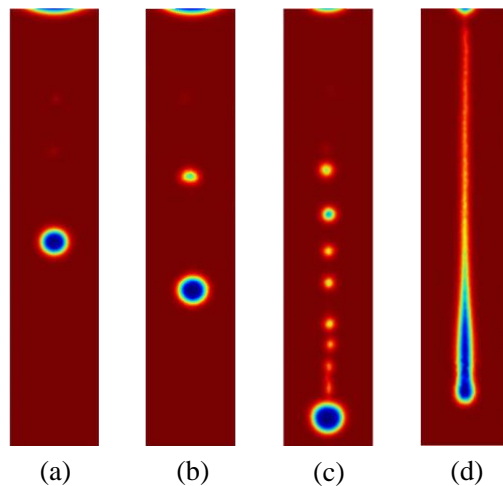

(a)　　　(b)　　　(c)　　　(d)

Fig. 6. Stability classification of the ejected fluid. (a) a single droplet (Class 1), (b) a major droplet with several satellites (Class 2), (c) a major droplet with a column of satellites (Class 3), and (d) a jet (Class 4).

Data shows that the speed variances have a large span from 0 to 19.414 m/s, and experience the same trend of all three types of nozzles. A larger droplet speed is reached by adopting larger ink density, lower ink viscosity, and smaller nozzle diameter.

Due to the higher proportion of inertial force, the liquid inside the channel owns more energy to overcome the surface energy at the nozzle, thus the droplet that pushed out has higher speed. Lower ink viscosity leads to less viscosity dissipation, which render more energy be converted into kinetic energy of droplet. According to the continuity equation, a nozzle with smaller diameter pushes out liquid with higher speed when the mass flow is constant. The average volume of the CT nozzle is relatively smaller compared with that of the circular and the Laval nozzles. Volume of the droplet is estimated at the breaking point of the jet so that the effect of the CT nozzle on reducing ink volume is relatively smaller compared with that of Fig. 5(a) whose volumes are obtained when droplets nearly reach the substrate. The stability trends of the circular nozzle and the CT nozzle are the same, which means the outlet shape of nozzle has negligible impact on the changes of the process instability that induced by other parameters. In Cases 4, 7 and 8, the Laval nozzle tends to weaken the droplet stability, which implies the strong influence of the nozzle's wall shape on the process instability.

Tables 5-7 present statistical analysis and optimal combination for droplet speed, volume and process stability, respectively. The parameters of k1-k3 indicate an averaged number of each level, like 9.739 located in the k1 row and the *A* column of Table 5, which represents the average speed of the cases of three Laval nozzles. R is the range of the average number, the larger of which represents stronger impact of the factors. Data shows that even the same factor has different impacts on the two kinds of improved nozzles. In Table 5, the order of influence on droplet speed when adopting the Laval nozzle is *D* (diameter), *A*(density), *B* (viscosity) and *C* (surface tension), while that is *D>B=C>A* when adopting the CT nozzle. Specifically, the optimal combinations for reaching the fastest speed are $A_3B_1C_3D_1$ and $A_3B_1C_1D_1$ for the Laval nozzle and

Table 7 Statistical analysis and optimal combination for process stability

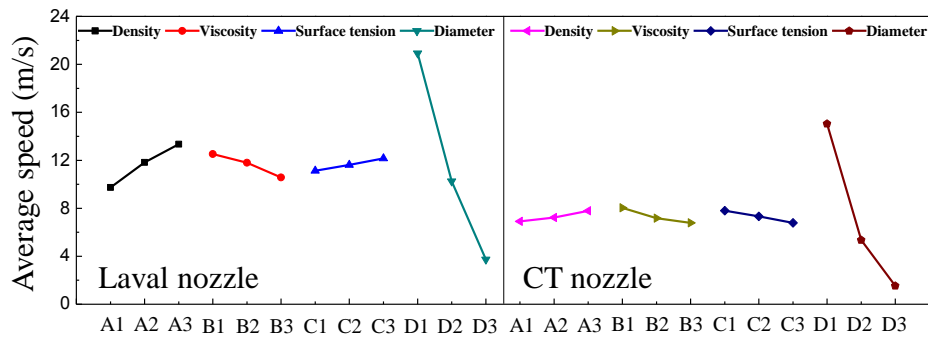| Parameters	Laval				CT			
	A	*B*	*C*	*D*	*A*	*B*	*C*	*D*
k1	2.667	3.667	3.333	4.000	2.667	3.000	3.000	4.000
k2	3.333	3.333	3.333	3.333	3.000	3.000	3.000	3.000
k3	3.667	2.667	3.000	3.000	3.000	2.667	2.667	1.667
R	1.000	1.000	0.333	0.333	0.333	0.333	0.333	2.333
Order	*C>D=A=B*				*D>A=B=C*			
Optimization	*A₁B₃C₃D₃*				*A₁B₃C₃D₃*			

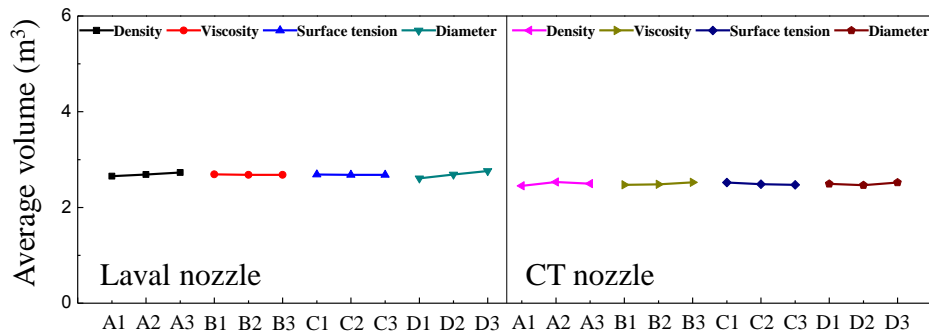**Fig. 7. Profiles of speed for four factors of the Laval and CT nozzles.**

Fig. 8. Profiles of volume for four factors of the Laval and CT nozzles.

the CT nozzle, respectively. Similarly, to obtain the smallest droplet volume through varying ink properties and nozzle diameter, the influential order is *D, A, B* and *C* for the Laval nozzle, the optimal combination for the Laval nozzle is $A_1B_{2/3}C_3D_1$, the influential order for the CT nozzle is *A, D, B, C*, and the optimal combination for the CT nozzle is $A_1B_1C_3D_2$. In addition, four factors have diverse effects on droplet stability. For the Laval nozzle, the influential order is *C>D=A=B*, and optimal combination is $A_1B_3C_3D_3$. For the CT nozzle, the influential order is *D>A=B=C*, and optimal combination is the same as that of the Laval nozzle.

The effects of four factors on droplet speed, volume and process stability are apparent by presenting the variances in Figs. 7-9. In addition, Tables 8 and 9 provide analysis results on the source of variance and significance test for Laval nozzle and CT nozzle, respectively. The squares of deviations of factors *SS* lie in the second column. Then, each variance of factors is defined as *MS = SS/df*, where *df* is the degree of freedom of each factors. *F*-test

can be expressed as $F = MS/M_{Total}$, whose value signifies the significance of factors in comparison to a given significance level (*α*). The expression of the confidence coefficient *θ* is *θ* = (1-*α*) × 100%. Here we choose *α* = 0.05 as the given significance level. Given that $F_{0.1}(2, 8) = 3.11$ and $F_{0.05}(2, 8) = 4.46$, if *F*-test of each factors lies in the range of 3.11 to 4.46, then its significance can be marked as "*", if it is less than 3.11, then this factor is marked as non-significant (ns). As presented above, diameter has the most significant effect on the droplet moving speed, the droplet volume and the process stability, which validate the results of Tables 5-7. The following conclusions by means of orthogonal analysis can be obtained. Firstly, to achieve faster droplets, both the Laval nozzle and the CT nozzle should adopt larger ink density, smaller ink viscosity and smaller nozzle diameter. A larger surface tension is conducive to improve speed for the Laval nozzle but is harmful for the CT nozzle. Secondly, the CT nozzle owns the merit of producing small volume droplet in average. Finally,
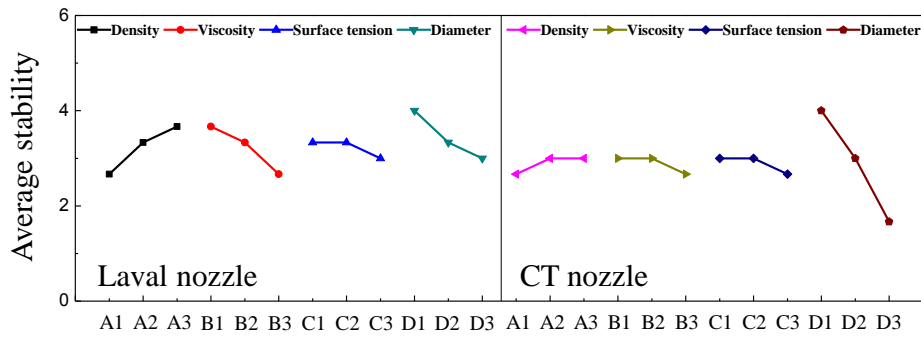
Fig. 9. Profiles of stability for four factors of the Laval and CT nozzles.

Table 8 Analysis results on the source of variance and significance test for Laval nozzle

Sources	*SS*	*df*	*MS*	*F*-test	*α*	*θ*/%	*significance*
$F_{0.1}(2, 8)=3.11$, $F_{0.05}(2, 8)=4.46$							
(a) For droplet moving speed							
A	19.64	2	9.82	0.164	0.05	95	ns
B	5.838	2	2.919	0.049	0.05	95	ns
C	1.597	2	0.7985	0.013	0.05	95	ns
D	452.065	2	226.0325	3.774	0.05	95	*
Total	479.14	8	59.8925				
(b) For droplet volume							
A	0.005	2	0.0025	0.500	0.05	95	ns
B	0.000	2	0.0000	0.000	0.05	95	ns
C	0.000	2	0.0000	0.000	0.05	95	ns
D	0.035	2	0.0175	3.500	0.05	95	ns
Total	0.04	8	0.0050				
(c) For process stability							
A	1.556	2	0.778	0.824	0.05	95	ns
B	1.556	2	0.778	0.824	0.05	95	ns
C	0.222	2	0.111	0.118	0.05	95	ns
D	4.222	2	2.111	2.235	0.05	95	ns
Total	7.560	8	0.945				

high ink viscosity, surface tension and nozzle diameter, as well as low ink density, are beneficial for enhancing stability for both of the two nozzles.

So far all choices are around optimizations of one aspect because the operating conditions that are beneficial for increasing the droplet speed may not be suitable for reducing the droplet volume or enhancing the process stability. Hereby, the parameter *Sc* that combines the droplet speed, the droplet volume and the process stability is introduced to obtain a comprehensive performance of the inkjet process.

Sc denotes a relative effect with the combination of the inkjet characteristics. A higher value of *Sc* (faster droplet speed, and/or lower droplet volume, and/or lower level of instability) signifies a better performance of the printing process, and vice versa.

The values of *Sc* are presented in the last column of Tables 2-4. Because the performance in single aspect may sacrifice in order to get a higher score in the comprehensive performance, none of the optimal combinations including improving the droplet speed, volume and the process stability reaches a high *Sc*. The highest *Sc* for droplet speed optimization is hard to evaluate because a spray process will emerge when trying to obtain an extreme high speed. *Sc* for the droplet volume

Table 9 Analysis results on the source of variance and significance test for CT nozzle

Sources	SS	df	MS	F-test	α	θ/%	significance
$F_{0.1}(2, 8)=3.11$, $F_{0.05}(2, 8)=4.46$							
(a) For droplet moving speed							
A	1.197	2	0.5985	0.016	0.05	95	ns
B	2.793	2	1.3965	0.038	0.05	95	ns
C	1.525	2	0.7625	0.021	0.05	95	ns
D	291.573	2	145.7865	3.926	0.05	95	*
Total	297.09	8	37.13625				
(b) For droplet volume							
A	0.009	2	0.0045	1.800	0.05	95	ns
B	0.004	2	0.0020	0.800	0.05	95	ns
C	0.003	2	0.0015	0.600	0.05	95	ns
D	0.004	2	0.0020	0.800	0.05	95	ns
Total	0.02	8	0.0025				
(c) For process stability							
A	0.222	2	0.111	0.100	0.05	95	ns
B	0.222	2	0.111	0.100	0.05	95	ns
C	0.222	2	0.111	0.100	0.05	95	ns
D	8.222	2	4.111	3.700	0.05	95	*
Total	8.89	8	1.11125				

optimization are at levels up to 1.978 ($A_1B_2C_3D_1$ of the Laval nozzle), and *Sc* for the process stability optimization are at levels up to 0.478 ($A_1B_3C_3D_3$ of the Laval nozzle). However, Sc can be increased to 2.096 as adopting the operating parameters in Case 5 of Table 3. Given that unilateral optimization has to sacrifice other performances, the combination of orthogonal method and *Sc* shows its significance in choosing proper nozzle structure and in designing inks in practice.

5. CONCLUSION

To improve performance of the inkjet technology, the droplet speed, volume and stability during the ejection process should be optimized. In the paper, the numerical simulation that is verified by experimental study is performed to examine the droplet movement after ejected from a piezoelectric driving nozzle. It is found that the Laval nozzle can increase the droplet speed for 140.6% compared to a general nozzle, and the CT nozzle can decrease the droplet volume up to 30.4%. The impacts of four operating factors, including ink density, viscosity, surface tension and nozzle diameter, on the droplet speed, volume and process stability for two chosen nozzles have been further investigated through orthogonal test method. Large ink density and surface tension, as well as small ink viscosity

and nozzle diameter, can boost the droplet speed for both nozzle structures, whereas only the CT shape nozzle has relatively strong effect on reducing droplet volume regardless of other parameters. High viscosity, surface tension and diameter as well as low density also contribute to an improved process stability. Optimal combinations for high speed, small volume and high process stability are obtained, respectively. Later a parameter *Sc* that combines the droplet speed, the droplet volume and the process stability is utilized for evaluating the comprehensive performance of inkjet process. It is determined that *Sc* for the droplet volume optimization are at levels up to 1.978, and for the process stability optimization are at levels up to 0.478. The conclusions provide important reference for nozzle structure design and ink preparation.

REFERENCES

Barenblatt, G. I. (1996). *Scaling, self-similarity, and intermediate asymptotics*. Cambridge University Press.

Castrejon-Pita, J. R., W. R. S. Baxter, J. Morgan, S. Temple, G. D. Martin and I. M. Hutchings (2013). Future, opportunities and challenges of inkjet technologies. *Atomization and Sprays* 23(6), 541–565.

Chen, A. U. and O. A. Basaran (2002). A new method for significantly reducing drop radius without reducing nozzle radius in drop-on-demand drop production. *Physics of Fluids*, 14(1), L1–L4.

Chen, H. H. and M. P. Brenner (2004). The Optimal Faucet. *Physical Review Letters*, *American Physical Society* 92(16), 166106.

Choi, I. H., Y. K. Kim, S. Lee,S. H. Lee, J. and Kim (2015). A Pneumatic Drop-on-Demand Printing System With an Extended Printable Liquid Range. *Journal of Microelectromechanical Systems*, 24(4), 768-770.

Eggers, J. (1993). Universal pinching of 3D axisymmetric free-surface flow. *Physical Review Letters*, *American Physical Society*, 71(21), 3458-3460.

Eggers, J. and T. F. Dupont, (1994). Drop formation in a one-dimensional approximation of the Navier–Stokes equation. *Journal of Fluid Mechanics*, Cambridge University Press, 262(1), 205.

Elrod, S. A., B. Hadimioglu, B. T. Khuri- Yakub, E. G. Rawson, E. Richley, C. F. Quate, N. N. Mansour and T. S. Lundgren (1989). Nozzleless droplet formation with focused acoustic beams. *Journal of Applied Physics*, 65(9), 3441-3447.

Fromm, J. E. (1984). *Numerical calculation of the fluid dynamics of drop-on-demand jets*. IBM Corp.

Hadimioglu, B., S. Elrod and R. Sprague (n.d.). Acoustic ink printing: an application of ultrasonics for photographic quality printing at high speed. *2001 IEEE Ultrasonics Symposium. Proceedings. An International Symposium (Cat. No.01CH37263)*, IEEE, 627-635.

Infanger, S., A. Haemmerli, S. Iliev, A. Baier, E. Stoyanov and J. Quodbach (2019). Powder bed 3D-printing of highly loaded drug delivery devices with hydroxypropyl cellulose as solid binder. *International Journal of Pharmaceutics* 555, 198-206.

Kastner, J., I. Gnatiuk, M. Wagner, D. Holzinger, V. Rudelstorfer, G. Hesser, A. Fuchsbauer and S. Hild (2019). Grinded nano-graphite inkjet inks for application in organic solar cells. *Nanotechnology* 30(4), 045601.

Keller, J. B., S. I. Rubinow and Y. O. Tu (1973). Spatial instability of a jet. *Physics of Fluids*, *American Institute of Physics* 16(12), 2052.

Khan, S., L. Lorenzelli and R. S. Dahiya (2015). Technologies for Printing Sensors and Electronics Over Large Flexible Substrates: A Review. *IEEE Sensors Journal* 15(6), 3164-3185.

Liao, Y., W. Liao, S. Chang, C. Hou, C. Tai, C. Su, Y. Hsu, M. Wu, R. Chou, Y. Lee, S. Lin, W. Lin, C. Chang, G. Haider, M. Kataria, P. K. Roy, K. P. Bera, C. R. PaulInbaraj, H. Hu, T. Lin and Y. Chen (2018). Inkjet- Printed Random Lasers. *Advanced Materials Technologies* 3(12), 1800214.

Lin, S. P. and R. D. Reitz (1998). Drop and spray formation from a liquid jet. *Annual Review of Fluid Mechanics*, 30(1), 85-105.

Martínez-Calvo, A., M. Rubio-Rubio and A. Sevilla (2018). The nonlinear states of viscous capillary jets confined in the axial direction. *Journal of Fluid Mechanics*, Cambridge University Press 834, 335-358.

McGuinness, P., W. Drenckhan and D. Weaire (2005). The optimal tap: three-dimensional nozzle design. *Journal of Physics D: Applied Physics* 38(18), 3382-3386.

Mishra, S., K. L. Barton, A. G. Alleyne, P. M. Ferreira and J. A. Rogers (2010). High-speed and drop-on-demand printing with a pulsed electrohydrodynamic jet. *Journal of Micromechanics and Microengineering*, IOP Publishing, 20(9), 095026.

Olsson, E. and G. Kreiss (2005). *A conservative level set method for two phase flow*. Academic Press Professional, Inc.

Olsson, E., G. Kreiss and S. Zahedi (2007). A conservative level set method for two phase flow II. *Journal of Computational Physics* 225(1), 785-807.

Peregrine, D. H. (1972). Equations for water waves and the approximations behind them. *Waves on beaches and resulting sediment transport* 95-121.

Reis, N. and B. Derby (2000). Ink Jet Deposition of Ceramic Suspensions: Modeling and Experiments of Droplet Formation. *MRS Proceedings*, 624, 65.

Rosati, G., M. Ravarotto, M. Scaramuzza, A. De Toni and A. Paccagnella (2019). Silver nanoparticles inkjet-printed flexible biosensor for rapid label-free antibiotic detection in milk. *Sensors and Actuators B: Chemical* 280, 280-289.

Shimobayashi, S. F., M. Tsudome and T. Kurimura (2018). Suppression of the coffee-ring effect by sugar-assisted depinning of contact line. *Scientific Reports* 8(1), 17769.

Silverbrook, K. (2011). *Inkjet nozzle assembly with low density suspended heater element*.

Tse, C. C. W. and P. J. Smith (2018). *Inkjet Printing for Biomedical Applications*. Humana Press, New York, NY, 107–117.

Wang, F. and T. Fang (2015). Liquid jet breakup for non-circular orifices under low pressures. *International Journal of Multiphase Flow Pergamon*, 72, 248–262.

Wijshoff, H. (2010). The dynamics of the piezo inkjet printhead operation. *Physics Reports*, 491(4-5), 77-177.

Wijshoff, H. (2018). Drop dynamics in the inkjet printing process. *Current Opinion in Colloid & Interface Science* 36, 20–27.

Zhang, B., X. Pei, P. Song, H. Sun, H. Li, Y. Fan, Q. Jiang, C. Zhou and X. Zhang (2018). Porous bioceramics produced by inkjet 3D printing: Effect of printing ink formulation on the ceramic macro and micro porous architectures control. *Composites Part B: Engineering* 155, 112–121.

Zhong, Y., H. Fang, Q. Ma and X. Dong (2018). Analysis of droplet stability after ejection from an inkjet nozzle. *Journal of Fluid Mechanics*, Cambridge University Press, 845, 378–391.